

Ising model for melt ponds on Arctic sea ice

Yi-Ping Ma¹, Ivan Sudakov², Courtenay Strong³, and Kenneth M. Golden^{4,*}

¹Northumbria University, Department of Mathematics, Physics, and Electrical Engineering, Newcastle upon Tyne, NE1 8ST, UK

²University of Dayton, Department of Physics, 300 College Park, SC 111, Dayton, Ohio 45469-2314, USA

³University of Utah, Department of Atmospheric Sciences, 135 S 1460 E Rm 819, Salt Lake City, Utah, 84112-0102, USA

⁴University of Utah, Department of Mathematics, 155 S 1400 E Rm 233, Salt Lake City, Utah 84112-0090, USA

*email: golden@math.utah.edu

Perhaps the most iconic feature of melting Arctic sea ice is the formation of distinctive, complex ponds on its surface during late spring. The evolution of melt ponds and their geometrical characteristics determines the albedo of sea ice, a key parameter in climate modeling^{1–5}. However, a theoretical understanding of this evolution, and predictions of geometrical features, have remained elusive. To address this fundamental problem in polar climate science, here we introduce a two dimensional random field Ising model for melt ponds. The ponds are identified as metastable states^{6–8} of the system, where the binary spin variable corresponds to the presence of melt water or ice on the sea ice surface. With only a minimal set of physical parameters, the model predictions agree very closely with observed power law scaling of the pond size distribution⁹ and critical length scale where melt ponds undergo a transition in fractal geometry¹⁰.

While snow and ice reflect most incident sunlight, melt ponds absorb most of it. The ponds largely control solar reflectance and transmittance of sea ice^{1–3,5}, which in turn impact the heat and mass balances of the ice cover and the partitioning of energy in the upper ocean and lower atmosphere. Typical pond configurations are shown in Fig. 1(a). It has been found⁴ that if a melt pond parameterization is included in climate model simulations, then predicted September ice volume from 1990 to 2007 is nearly 40% lower than in simulations which do *not* incorporate ponds, and is in much closer alignment with observations. Moreover, the yearly Arctic sea ice minimum can be accurately forecasted from melt pond area in spring⁵. The impact of melt pond evolution extends into the biosphere as well^{11,12}, where the ponds act as *windows* for light to shine into the upper ocean, affecting Arctic marine ecology.

There has been significant progress on the development of numerical models of melt pond evolution^{1,3–5}. However, a fundamental theory of melting sea ice which accounts for observed pond characteristics has been lacking. Here we look toward statistical physics, and the Ising model in particular^{13,14}, to develop such a theory. We envision surface patches or *pixels* of ice or melt water as collectively influenced by an external forcing field, and interacting only with their nearest neighbors.

A central issue in climate science is *linkage of scales* – that is, how can knowledge of small scale local interactions be used to predict *macroscopic* behavior relevant to large scale, coarse-grained models? This is the type of question that is addressed in statistical physics^{13,14} and homogenization for composite materials^{15,16}, where powerful methods of calculating macroscopic behavior from “microscopic” laws or microstructural information have been developed. Indeed, an Ising model for tropical convection was developed¹⁷ to represent unresolved features in the atmosphere. Here we employ such methods to represent a critically important unresolved feature in the polar marine environment.

First, we recall the most general form of the Ising free energy,

$$\mathcal{H} = - \sum_i H_i s_i - \sum_{\langle i,j \rangle} J_{ij} s_i s_j, \quad (1)$$

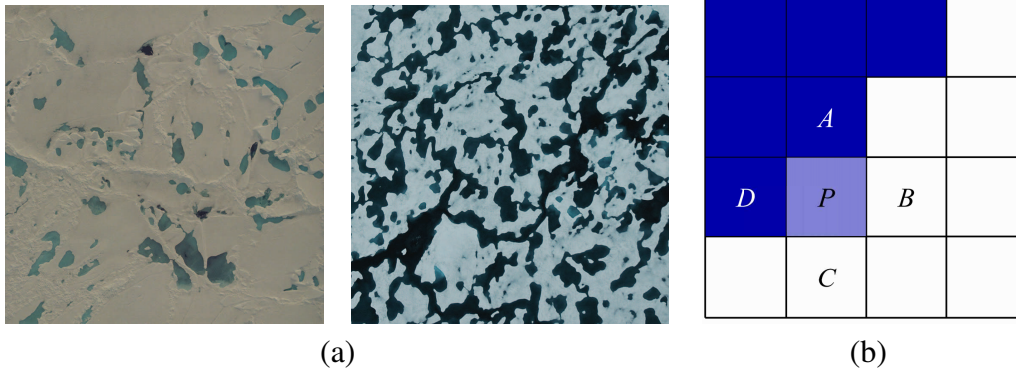


Figure 1. Melt pond configurations and the update step in Glauber dynamics. (a) Helicopter photos of melt ponds on Arctic sea ice in the western Beaufort Sea (courtesy of D. Perovich). On the left, each side of this 15 July 1998 photo is 826 meters; on the right, each side of this 14 August 2005 photo is 193 meters. (b) Illustration of an update step in Glauber single spin-flip dynamics of the Ising model. Here each site i is assigned a pre-melt ice height h_i , and colored dark blue for water ($s_i = +1$) and white for ice ($s_i = -1$). Site P , to be updated, is adjacent to two water sites A and D , and two ice sites B and C . To describe the tendency for water to fill troughs, we require that $s_P = +1$ if $h_P < 0$, and -1 otherwise.

where i ranges over a two dimensional square lattice with periodic boundary conditions, and $\langle i, j \rangle$ denotes nearest neighbors. In our model the state variable is a binary (or spin) variable s_i such that $s_i = +1$ corresponds to absorptive melt water on the surface of our pixelated model sea ice floe and $s_i = -1$ corresponds instead to reflective ice or snow on the surface. The parameters H_i and J_{ij} represent the external magnetic field and coupling constants, respectively. In addition, a temperature T can be defined which controls the strength of thermal fluctuations, but here we set $T = 0$ assuming that environmental noise does not significantly influence melt pond formation.

To describe nontrivial spin clustering at zero temperature, the H_i and/or J_{ij} are chosen as random variables; the resulting models are collectively known as disordered Ising models¹⁸. In particular, one recovers the classical random field Ising model (RFIM) if the H_i are independent random variables and the $J_{ij} = J$ are constant. At zero temperature, the system is usually assumed to follow Glauber single spin-flip dynamics¹⁹: at each update step, the flip is accepted if \mathcal{H} decreases and rejected if \mathcal{H} increases. The system eventually converges to a local minimum of \mathcal{H} , known as a metastable state.

Metastable states are especially relevant to physical systems near phase transitions, including super-cooled liquids²⁰ and atmospheric aerosol particles²¹. For disordered Ising models they have been realized experimentally in, for example, doped manganites²² and colossal magnetoresistive manganites²³. Despite their importance, metastable states are not completely understood theoretically¹⁹, with analytical results largely restricted to 1D²⁴ and many intricate issues remaining in 2D²⁵.

The key factor controlling melt pond configurations is the pre-melt ice topography, represented by random variables h_i . In the spirit of creating order from disorder, these variables are assumed to be independent Gaussian with zero mean and unit variance. The lattice constant $a = 0.85$ m is specified as the length scale above which important spatially correlated fluctuations occur in the power spectrum of sea ice topography (see Supplementary Methods). We use the following update rule for Glauber dynamics, depending on whether there is a majority among the four neighbors of a chosen site. If a majority exists, the site is updated to align with the majority because of heat diffusion between neighboring sites. Otherwise, we introduce a *tiebreaker* rule that describes the tendency for water to fill troughs: the chosen site is updated to ice if its pre-melt ice height is positive, and water otherwise; see Fig. 1(b). Note that this

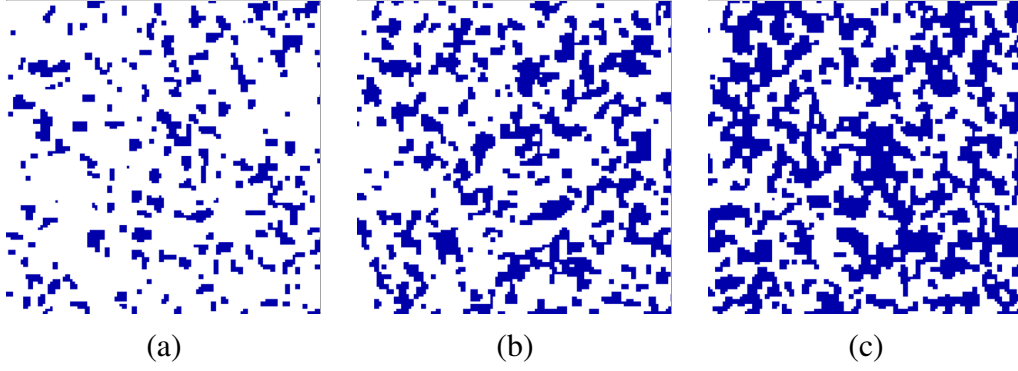


Figure 2. Melt ponds as metastable *islands* of like spins in our random field Ising model.

Simulation results are shown for metastable states of the RFIM at $H = 0$ and $J = 5$. The output spin configurations are shown on a 128×128 portion of the 1024×1024 lattice with (a) $F_{out} = 0.15$; (b) $F_{out} = 0.30$; (c) $F_{out} = 0.45$. Pixels are colored blue for water ($s_i = +1$) and white for ice ($s_i = -1$).

update rule does not depend on any parameters other than h_i .

The above update rule can be restated as minimizing the classical RFIM free energy^{6–8}

$$\mathcal{H} = \sum_i (h_i - H) s_i - \sum_{\langle i, j \rangle} J s_i s_j, \quad (2)$$

with the uniformly applied field $H = 0$ and the coupling constant $J \rightarrow +\infty$; see Supplementary Methods for a brief discussion of the $H \neq 0$ case. To facilitate comparison with geophysical observations, the order parameter will be taken as the pond fraction F , which is defined as the fraction of up-spins and therefore related to the magnetization M by $F = (M + 1)/2$. At $J = 0$, there is a unique metastable state given by $s_i = +1$ if $h_i < H$, and $s_i = -1$ if $h_i > H$. This process can only yield the correct melt pond geometry if the random variables h_i are highly correlated²⁶. As J increases, metastable states appear²⁷ at a wider range of pond fractions, with the entire range $F \in [0, 1]$ covered for large enough J .

Below we present numerical results for the zero temperature Glauber dynamics of the RFIM, with 10 Monte Carlo steps used for each simulation and the lattice size taken to be 1024×1024 . The input spin configurations s_i are independent binary variables that equal $+1$ with probability F_{in} and -1 with probability $1 - F_{in}$, where F_{in} denotes the input pond fraction. Note that these variables are uncorrelated with the h_i . Following a random update sequence, Glauber dynamics eventually yield a metastable state with output pond fraction F_{out} . Fig. 2 shows the output configurations with $F_{out} = 0.15, 0.30$, and 0.45 . This metastability is consistent with previous findings from a dynamical systems analysis²⁸.

The up-spin clusters in Fig. 2(c) at $F_{out} = 0.45$ correspond to well developed melt ponds¹⁰. Fig. 3(a) shows the log-log plot of the perimeter P versus the area A for these clusters (shown in physical units as Pa and Aa^2). Fig. 3(b) shows the pond size distribution function $\text{prob}(A)$. It exhibits power law scaling $\text{prob}(A) \sim A^\zeta$ with the exponent $\zeta = -1.58 \pm 0.03$ for pond areas in the range $10 \text{ m}^2 < A < 1,000 \text{ m}^2$, in excellent agreement with the observed value⁹ of about $-3/2$.

A key feature of multi-cluster systems is the tendency for smaller clusters to have simple shapes and larger clusters to have complex shapes. This onset of complexity can be quantified by an increase in the fractal dimension D , defined in terms of the perimeter P and the area A as $P \sim \sqrt{A}^D$. To find the critical area above which shapes do not remain simple, we choose the smallest possible P for each A , or equivalently the lower edge of the cluster of points in the (A, P) -plane. Fig. 3(c) shows the function $D(A)$ computed for our model, illustrating the fractal dimension transition from 1 to 2 around a critical area

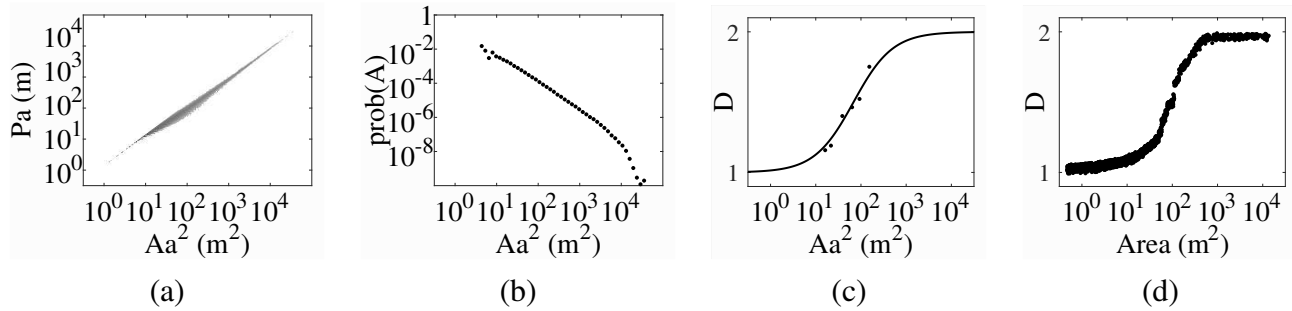


Figure 3. Geometrical characteristics of Ising model melt ponds. Simulation data in this figure are for the up-spin clusters in Fig. 2(c). (a) Log-log plot of the perimeter P versus the area A , rendered as a (rescaled) density plot. (b) Log-log plot of the pond size distribution function $\text{prob}(A)$, with bin size 0.2 and very small ponds excluded. (c) Plot of the fractal dimension D as a function of A (log scale) for our melt pond Ising model. The individual points show the local fractal dimensions (computed from the lower edge of the convex hull of the data points in panel (a)) within the range $10 \text{ m}^2 < A < 1,000 \text{ m}^2$. (d) (Reproduced¹⁰ with permission.) Plot of the fractal dimension as a function of area (log scale) based on image analysis of real melt ponds¹⁰. For panels (a)-(c), to compare with observations, A and P are shown in physical units with the lattice constant $a = 0.85 \text{ m}$, and the number of lattice sites is increased to 8192×8192 to improve the statistics.

A_c . Fitting a suitable smooth function to the data points²⁶, we find that the transition happens around the inflection point $A_c a^2 \approx 70 \text{ m}^2$. This predicted value agrees well with the observed value¹⁰ of about 100 m^2 , as reproduced in Fig. 3(d). The width of the transition regime in $\log(A)$ in Fig. 3(c) also agrees well with Fig. 3(d). Finally, Supplementary Fig. 2 displays another quantifier of the onset of complexity that accounts for the entire cluster of points in the (A, P) -plane. It yields the same critical area as before, $A_c a^2 \approx 70 \text{ m}^2$.

Minimal models such as the RFIM necessarily have limitations. In particular, the RFIM has a percolation threshold very close to 0.5 at $H = 0$ (see Supplementary Methods). This threshold decreases as H decreases, but likely always exceeds the value for real melt ponds. This discrepancy may be attributed to unresolved processes at smaller scales, and/or the observed pre-melt ice topography being spatially correlated rather than completely random (see Supplementary Fig. 1). We anticipate that, based on a significant amount of observational data, a detailed scheme for choosing the initial spin configuration and update sequence may be formulated. See also Supplementary Methods for possible modifications to the update rule with an alternative free energy yielding similar predictions.

The interpretation of complex Arctic melt ponds in terms of a simple disordered system may well advance our ability to model the future trajectory of the Arctic sea ice pack, e.g., through parameterizations in global climate models²⁹. In addition, the statistical physics approach developed here may be generalizable to other systems near the transition point between ice and water, such as permafrost tundra lakes³⁰.

References

1. Scott, F. & Feltham, D. L. A model of the three-dimensional evolution of Arctic melt ponds on first-year and multiyear sea ice. *J. Geophys. Res.* **115**, C12064 (2010).
2. Perovich, D. K. & Polashenski, C. Albedo evolution of seasonal Arctic sea ice. *Geophys. Res. Lett.* **39**, L08501 (2012).

3. Polashenski, C., Perovich, D. & Courville, Z. The mechanisms of sea ice melt pond formation and evolution. *J. Geophys. Res.* **117**, C01001 (2012).
4. Flocco, D., Schroeder, D., Feltham, D. L. & Hunke, E. C. Impact of melt ponds on Arctic sea ice simulations from 1990 to 2007. *J. Geophys. Res.* **117**, C09032 (2012).
5. Schröder, D., Feltham, D. L., Flocco, D. & Tsamados, M. September Arctic sea-ice minimum predicted by spring melt-pond fraction. *Nat. Clim. Change* **4**, 353–357 (2014).
6. Andelman, D. & Joanny, J.-F. Metastability in the random-field Ising model. *Phys. Rev. B* **32**, 4818–4821 (1985).
7. Grant, M. & Gunton, J. D. Metastable states in the random-field Ising model. *Phys. Rev. B* **35**, 4922–4928 (1987).
8. Perez-Reche, F. J., Rosinberg, M. L. & Tarjus, G. Numerical approach to metastable states in the zero-temperature random-field Ising model. *Phys. Rev. B* **77**, 064422 (2008).
9. Perovich, D. K., Tucker, W. B. & Ligett, K. Aerial observations of the evolution of ice surface conditions during summer. *J. Geophys. Res.* **107**, C000449 (2002).
10. Hohenegger, C., Alali, B., Steffen, K. R., Perovich, D. K. & Golden, K. M. Transition in the fractal geometry of Arctic melt ponds. *The Cryosphere* **6**, 1157–1162 (2012).
11. Arrigo, K. R. *et al.* Massive phytoplankton blooms under Arctic sea ice. *Science* **336**, 1408–1408 (2012).
12. Nicolaus, M., Katlein, C., Maslanik, J. & Hendricks, S. Changes in Arctic sea ice result in increasing light transmittance and absorption. *Geophys. Res. Lett.* **39**, L24501 (2012).
13. Yeomans, J. M. *Statistical Mechanics of Phase Transitions* (Clarendon Press, 1992).
14. Christensen, K. & Moloney, N. R. *Complexity and Criticality* (Imperial College Press, 2005).
15. Milton, G. W. *The Theory of Composites*. Cambridge Monographs on Applied and Computational Mathematics, Vol. 6 (Cambridge University Press, 2002).
16. Torquato, S. *Random Heterogeneous Materials: Microstructure and Macroscopic Properties* (Springer-Verlag, 2002).
17. Khouider, B., Majda, A. J. & Katsoulakis, M. A. Coarse-grained stochastic models for tropical convection and climate. *Proc. Natl Acad. Sci. USA* **100**, 11941–11946 (2003).
18. Young, A. P. *Spin Glasses and Random Fields* (World Scientific, 1998).
19. Krapivsky, P. L., Redner, S. & Ben-Naim, E. *A Kinetic View of Statistical Physics* (Cambridge University Press, 2010).
20. Büchner, S. & Heuer, A. Metastable states as a key to the dynamics of supercooled liquids. *Phys. Rev. Lett.* **84**, 2168–2171 (2000).
21. Rood, M., Shaw, M., Larson, T. & Covert, D. Ubiquitous nature of ambient metastable aerosol. *Nature* **337**, 537–539 (1989).
22. Moreo, A., Mayr, M., Feiguin, A., Yunoki, S. & Dagotto, E. Giant cluster coexistence in doped manganites and other compounds. *Phys. Rev. Lett.* **84**, 5568–5571 (2000).
23. Wu, W. *et al.* Magnetic imaging of a supercooling glass transition in a weakly disordered ferromagnet. *Nat. Mater.* **5**, 881–886 (2006).

24. Derrida, B. & Gardner, E. Metastable states of a spin glass chain at 0 temperature. *J. de Phys.* **47**, 959–965 (1986).
25. Newman, C. & Stein, D. Metastable states in spin glasses and disordered ferromagnets. *Phys. Rev. E* **60**, 5244–5260 (1999).
26. Bowen, B., Strong, C. & Golden, K. M. Modeling the fractal geometry of Arctic melt ponds using the level sets of random surfaces. *J. Fract. Geom.*, **in press** (2017).
27. Wu, Y. & Machta, J. Ground states and thermal states of the random field Ising model. *Phys. Rev. Lett.* **95**, 137208 (2005).
28. Sudakov, I., Vakulenko, S. A. & Golden, K. M. Arctic melt ponds and bifurcations in the climate system. *Commun. Nonlinear Sci. Numer. Simul.* **22**, 70 – 81 (2015).
29. Flocco, D., Feltham, D. L. & Turner, A. K. Incorporation of a physically based melt pond scheme into the sea ice component of a climate model. *J. Geophys. Res.* **115**, C08012 (2010).
30. Sudakov, I. & Vakulenko, S. A. A mathematical model for a positive permafrost carbon-climate feedback. *IMA J. Appl. Math.* **80**, 811–824 (2015).

Acknowledgments

We gratefully acknowledge support from the Division of Mathematical Sciences and the Division of Polar Programs at the U.S. National Science Foundation (NSF) through Grants DMS-1009704, ARC-0934721, DMS-0940249, DMS-1413454, and DMS-0940262. We are also grateful for support from the Office of Naval Research (ONR) through Grant N00014-13-10291. Y.M. acknowledges support from a Vice Chancellor’s Research Fellowship at Northumbria University. I.S. acknowledges support from the RFBR under the Grant #16-31-60070 mol_a.dk. Finally, we would like to thank the NSF Math Climate Research Network (MCRN) for their support of this work.

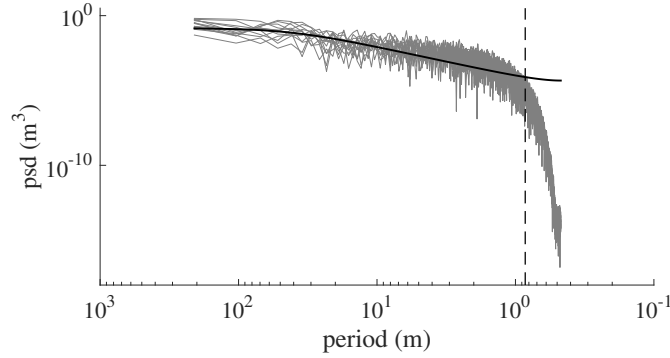
Y.M., I.S., C.S., and K.G. proposed the model. Y.M. and C.S. performed the numerical work. All authors contributed significantly to writing the manuscript.

Competing financial interests

The authors declare no competing financial interests.

Supplementary Methods

Lattice constant. The lattice constant a must be small relative to the 10-20 m length scales prominent in sea ice and snow topography³¹. We set $a = 0.85$ m as the length above which the power spectral density (psd) of observed snow topography exceeds a null red noise spectrum (Supplementary Fig. 1). For this calculation, we used 13 radar transects collected during the Surface Heat Budget of the Arctic Ocean (SHEBA) project³². To estimate the psd via the Welch modified periodogram, we calculated the power spectrum for each transect with a Hanning window and 50% segment overlap, and then averaged the results across the transects. We calculated the corresponding null red noise spectrum based on lag-one spatial autocorrelation³³ averaged across the transects.



Supplementary Figure 1. Snow depth power spectral density (gray curve) with corresponding null red noise spectrum (black curve). The lattice constant $a = 0.85$ m is indicated by a vertical dashed line.

Alternative quantifier of the onset of complexity. To account for the entire cluster of points in the (A, P) -plane in Fig. 3(a), we define a new quantifier of the onset of complexity as the variance σ of $\log(P)$, hereafter referred to as the *elasticity*. As shown in Supplementary Fig. 2, there exists a critical area A_c such that $\sigma(\log(P))$ increases with $\log(A)$ for simple ponds with $A < A_c$, and decreases with $\log(A)$ for complex ponds with $A > A_c$. The onset of complexity may then be identified with maximum elasticity, which occurs at $A_c a^2 \approx 70$ m². This coincides with the critical area determined from Fig. 3(c) by the inflection point in the best fit.

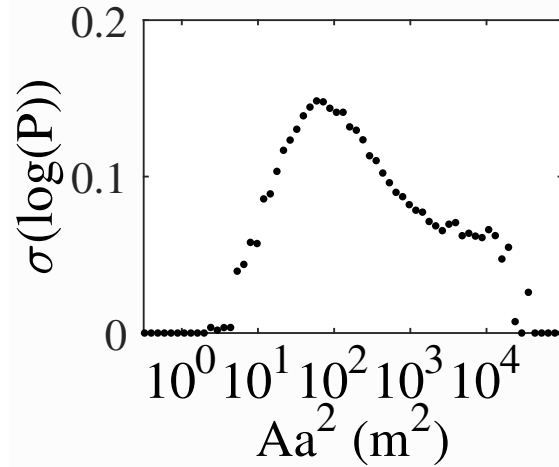
Percolation threshold and correlation length exponent. For a two dimensional square lattice with occupation probability p , the site-site correlation function $g(r_i, r_j)$ gives the probability that a site at r_j is a member of the same cluster as a site at r_i . The function g is assumed to decay with large distance $d = |r_i - r_j|$ according to

$$g(d) \sim \exp\left(-\frac{d}{\xi(p)}\right), \quad (\text{S1})$$

where $\xi(p)$ is referred to as the correlation length. Theory indicates that $\xi(p)$ should obey

$$\ln \xi(p) \sim -\nu \ln(|p - p_c|), \quad p \rightarrow p_c^-, \quad (\text{S2})$$

where $\nu = 4/3$ is the universal critical exponent in two dimensions and p_c is the percolation threshold. For the two-dimensional square site lattice, $p_c \approx 0.59274621$ ³⁴. For the RFIM, analysis of 5,000 model realizations on 1024×1024 lattices yields a value close to $p_c = 0.5$ (Fig. 3a), with correlation lengths



Supplementary Figure 2. Plot of the variance $\sigma(\log(P))$ as a function of A (log scale), with bin size 0.2. The maximum happens at $A_c a^2 \approx 70 \text{ m}^2$.

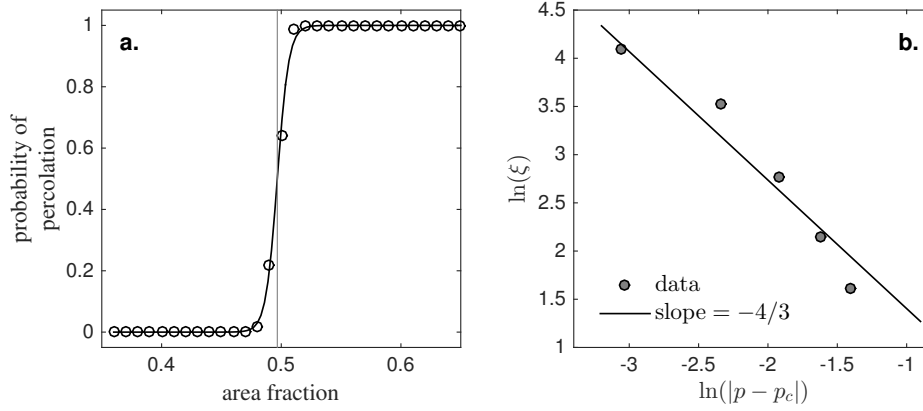
aligning reasonably with the universal exponent $\nu = 4/3$ (Fig. 3b). This result indicates that the spatial correlation structure of melt ponds in this model is sufficiently short-ranged so that the system falls within a standard universality class³⁵.

Time scale. The time scale for melt pond formation can be generally identified with the typical time taken to flip a spin in Glauber dynamics. After the RFIM decides that a spin flip is energetically favorable, we assume that the actual spin-flip process is facilitated by radiation balance³⁶. The incoming shortwave radiation is $\text{ISR} = Q(1 - \alpha)$, where $Q = 460 \text{ W} \cdot \text{m}^{-2}$ is the mean solar insolation during polar summer, and α is the surface albedo, 0.1 for water and 0.5 for ice. The outgoing longwave radiation is $\text{OLR} = \sigma T^4$, where now $\sigma = 5.67 \times 10^{-8} \text{ W} \cdot \text{m}^{-2} \text{K}^{-4}$ is the Stefan-Boltzmann constant, and T is the surface temperature, approximately 273 K for both water and ice. Therefore the rate of heat loss for ice is $R_i = \text{OLR} - \text{ISR} = 85 \text{ W} \cdot \text{m}^{-2}$, and the rate of heat gain for water is $R_w = \text{ISR} - \text{OLR} = 99 \text{ W} \cdot \text{m}^{-2}$. On the other hand, the energy per unit area required for freezing a water column or melting an ice column is $E = L\rho h$, where $L = 3.34 \times 10^5 \text{ J} \cdot \text{kg}^{-1}$ is the latent heat of fusion, $\rho = 1 \times 10^3 \text{ kg} \cdot \text{m}^{-3}$ is the density of water or ice (taken to be the same for simplicity), and $h = 0.3 \text{ m}$ is a realistic value for the height of the active layer. Therefore, the time intervals needed to freeze a water site or to melt an ice site are, respectively, $t_{w \rightarrow i} = E/R_i = 14$ days and $t_{i \rightarrow w} = E/R_w = 12$ days, both of which are reasonable, given this rough estimation.

Nonzero uniformly applied field. Let us choose $H \neq 0$ and keep $J \rightarrow +\infty$ in the RFIM given by Eq. (2). Then the tiebreaker rule for a chosen site i changes to $s_i = +1$ if $h_i < H$, and $s_i = -1$ if $h_i > H$, which favors ice for $H < 0$ and water for $H > 0$. Here we only consider two limiting cases when the tiebreaker rule completely favors ice or water: (I) $0 \ll -H \ll J$; (II) $0 \ll H \ll J$. In these cases, the random field h_i does not affect the kinetics, so the RFIM reduces to the classical Ising model without disorder,

$$\mathcal{H} = -H \sum_i s_i - J \sum_{\langle i,j \rangle} s_i s_j. \quad (\text{S3})$$

The corresponding metastable states are known as Wulff droplets³⁷. In case (I) the up-spin clusters are more elongated, and the percolation threshold is below 0.5. In case (II) the up-spin clusters are more



Supplementary Figure 3. (a) Probability of percolation as a function of area fraction. The curve is a hyperbolic tangent fit with inflection point close to 0.5 indicating the percolation threshold p_c . (b) Comparison of output from the Ising model (filled circles) to the line with slope $-\nu = -4/3$ given by the universal correlation length exponent ν .

circular, and the percolation threshold is above 0.5. These geometrical features afforded by varying H (and possibly also J) provide additional prospects to describe detailed shapes of real melt pond patterns.

Alternative update rule and free energy. Let us retain the RFIM update rule when a majority exists among the neighboring sites, but adopt the following tiebreaker rule: the chosen site is updated to ice if its pre-melt ice height is larger than the average between the two neighboring ice sites, and water otherwise. For example, in Fig. 1(b) we require that $s_P = +1$ if $h_P < (h_B + h_C)/2$, and -1 otherwise. This new update rule can be restated as minimizing an interfacial energy between water and ice: if a water site i neighbors an ice site j , then a penalty $W - h_j$ is imposed, where $W \gg 0$ is a constant. The total free energy \mathcal{H} can then be written in two equivalent forms,

$$\mathcal{H} = \sum_{\substack{\langle i,j \rangle: \\ s_i > 0, s_j < 0}} (W - h_j) \equiv \sum_i s_i \Delta_i h - \sum_{\langle i,j \rangle} \frac{1}{2} s_i s_j (W - \Omega_{ij} h), \quad (\text{S4})$$

where Δ_i and Ω_{ij} represent, respectively, the discrete Laplacian at site i and the average between sites i, j ,

$$\Delta_i h \equiv h_i - \frac{1}{4} \sum_{j: \langle i,j \rangle} h_j, \quad \Omega_{ij} h \equiv \frac{1}{2} (h_i + h_j). \quad (\text{S5})$$

The new “effective” random fields $\Delta_i h$, being the curvature of h_i , are more correlated than the h_i by themselves. As a result, at output pond fraction $F_{out} = 0.45$, the critical area for the transition in fractal dimension and the critical area for maximum elasticity are both $A_c a^2 \approx 90 \text{ m}^2$. The corresponding power law scaling exponent for the pond size distribution is $\zeta = -1.57 \pm 0.03$. It may be interesting to compare these geometrical characteristics with classical ferromagnetic random bond Ising models³⁸.

References

31. Petrich, C. *et al.* Snow dunes: A controlling factor of melt pond distribution on Arctic sea ice. *J. Geophys. Res.* **117**, C09029 (2012).

32. Sturm, M., Holmgren, J. & Perovich, D. K. Winter snow cover on the sea ice of the Arctic Ocean at the Surface Heat Budget of the Arctic Ocean (SHEBA): Temporal evolution and spatial variability. *J. Geophys. Res.* **107**, C000400 (2002).
33. Gilman, D. L., Fuglister, F. J. & Mitchell, J. M. On the power spectrum of “red noise”. *J. Atmos. Sci.* **20**, 182–184 (1963).
34. Newman, M. E. J. & Ziff, R. M. Efficient Monte Carlo algorithm and high-precision results for percolation. *Phys. Rev. Lett.* **85**, 4104–4107 (2000).
35. Isichenko, M. B. Percolation, statistical topography, and transport in random media. *Rev. Mod. Phys.* **64**, 961–1043 (1992).
36. Pierrehumbert, R. T. *Principles of Planetary Climate* (Cambridge University Press, 2010).
37. Schonmann, R. H. & Shlosman, S. B. Wulff droplets and the metastable relaxation of kinetic Ising models. *Commun. Math. Phys.* **194**, 389–462 (1998).
38. Jacobs, A. & Coram, C. Ferromagnetic random-bond Ising model: Metastable states and complexity of the energy surface. *Phys. Rev. B* **36**, 3844–3850 (1987).